Degenerate RFID Channel Modeling for Positioning Applications

Ales POVALAC[1], Klaus WITRISAL[2], Jiri SEBESTA[1]

[1]Dept. of Radio Electronics, Brno University of Technology, Purkynova 118, 612 00 Brno, Czech Republic
[2]Signal Processing and Speech Comm. Laboratory, Graz Univ. of Technology, Inffeldgasse 16c/EG, A-8010 Graz, Austria

ales.povalac@phd.feec.vutbr.cz, witrisal@tugraz.at, sebestaj@feec.vutbr.cz

Abstract. *This paper introduces the theory of channel modeling for positioning applications in UHF RFID. It explains basic parameters for channel characterization from both the narrowband and wideband point of view. More details are given about ranging and direction finding. Finally, several positioning scenarios are analyzed with channel models developed. All the described models use a degenerate channel, i.e. combined signal propagation from the transmitter to the tag and from the tag to the receiver.*

Keywords

RFID, UHF, channel modeling, ranging, FD-PDoA.

1. Introduction to RFID Localization

The communication range is pertinent to the concept of RFID transmission. It strongly depends on tag orientation, obstacles, environmental attenuation, and other local circumstances. A typical reading range of 2 m (using 0.5 W RF power) can drop to a tenth, as well as increase several times [1]. This variability of range is currently one of the key issues in RFID technology. A precise definition of the reading area is necessary in many applications, e.g. in a typical setup of parallel RFID gates in a warehouse.

Unfortunately, the industrial environment produces a really challenging RFID channel from the point of multipath propagation. This effect is desirable for tag reading, as it allows communication between tag and reader even if there is no direct line of sight. On the other hand, a considerable fading margin is needed to ensure detection of all RFID tags within the read volume while undesired reads of tags outside the read zone are hard to avoid. Furthermore, multipath propagation seriously damages the ranging information, which can be otherwise extracted from the direct signal in quite a simple way.

The most common method of distance measurement is based on received signal strength (RSS). Although this method is implemented in some way on almost all RFID readers, the accuracy is usually not sufficient for reasonable range estimation because it is strongly affected by the propagation environment [2].

This paper explains basic channel parameters and proposes several positioning scenarios. The spatial and frequency analysis of the RFID channel based on models with various levels of propagation complexity is provided.

2. Overview of RFID Channel Models

The wireless channel with multipath propagation can be characterized using its channel impulse response (CIR), i.e. the response of the tapped delay line channel model to the Dirac pulse. The general CIR is a time-variant function, which also depends on environment, RX/TX position, polarization, etc. For known positions $\vec{p}_{TX}, \vec{p}_{RX}$ of transmitter (TX) and receiver (RX), respectively, it is possible to simplify the CIR to $h(\vec{p}_{TX}, \vec{p}_{RX}, \tau)$, where τ is the propagation delay [3]. The CIR itself is a complex-valued function, it is therefore better to plot its squared magnitude, i.e. power delay profile (PDP):

$$S(\vec{p}_{TX}, \vec{p}_{RX}, \tau) = |h(\vec{p}_{TX}, \vec{p}_{RX}, \tau)|^2. \tag{1}$$

The discrete PDP is characterized by individual taps in the delay dimension, with the tap i specified by its delay τ_i and power P_i. A physical representation of the PDP with only one path is shown in Fig. 1(a). This unobstructed direct path is called the line-of-sight (LOS) component. In multipath propagation, several other paths are added, called non-line-of-sight (NLOS) components, e.g. Fig. 1(b).

(a) PDP of LOS only   (b) PDP of LOS and two reflections
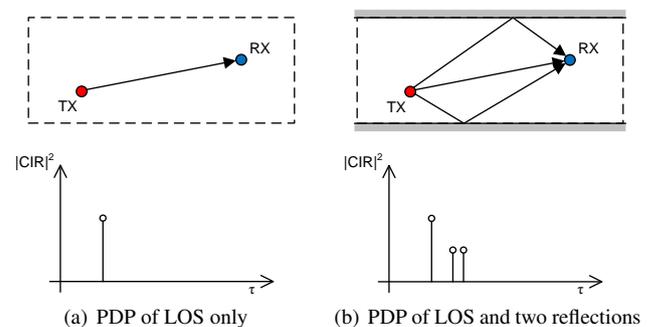
Fig. 1. Physical representation of power delay profile.
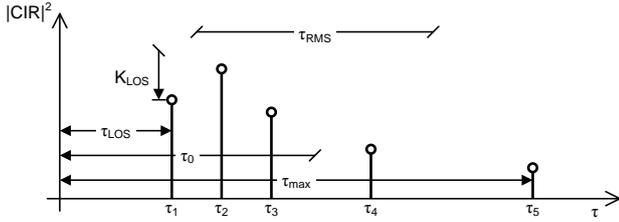
Fig. 2. Channel parameters in power delay profile.

The following channel parameters can be defined using the PDP (see Fig. 2) with *n* taps according to [3], [4]:

- **Mean delay**, τ_0: the average delay weighted by power defined as:

$$\tau_0 = \frac{1}{P_T} \sum_{i=1}^{n} P_i \tau_i \quad \text{where} \quad P_T = \sum_{i=1}^{n} P_i. \qquad (2)$$

- **LOS delay**, τ_{LOS}: the delay corresponding to the direct LOS path.

- **Maximum excess delay**, τ_{max}: the last significant delay.

- **RMS delay spread**, τ_{RMS}: the spread of the taps, considering both relative powers and delays of the taps, defined as:

$$\tau_{RMS} = \sqrt{\frac{1}{P_T} \sum_{i=1}^{n} P_i \tau_i^2 - \tau_0^2}. \qquad (3)$$

- **Ricean K-factor**, K_{LOS}: the power ratio between the direct (LOS) path and scattered (NLOS) multipath components.

The LOS delay τ_{LOS} is the most important parameter for ranging, as it directly defines the distance between RX and TX. Unfortunately, to isolate this component from the others in a strong multipath environment with large τ_{RMS}, it is necessary to use a large measurement bandwidth, i.e. an ultra-wideband (UWB) system. The spatial resolution of a UWB is in an ideal case given by:

$$d_{res} = \frac{c}{2B} \qquad (4)$$

where *c* is the speed of light and *B* is the signal bandwidth. The direct LOS path does not have to be the strongest path in a severe multipath environment ($K_{LOS} < 0$ dB).

Another channel characterization approach is based on channel transfer function (CTF), which is the inverse Fourier transform of the CIR. The CTF provides a complex channel gain of a given frequency and therefore can be measured in a relatively simple way. An example of the CTF corresponding to the CIR with three components is shown in Fig. 4.
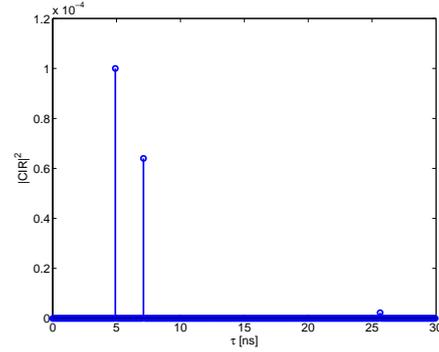
Fig. 3. Example CIR for an enviroment with three propagation paths.
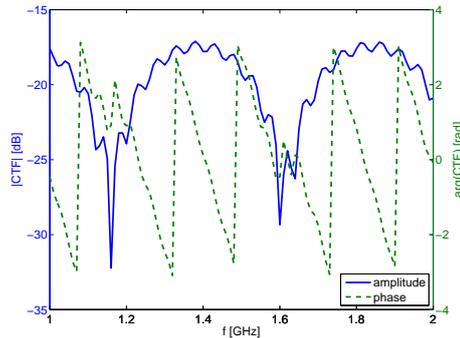
Fig. 4. Corresponding CTF (amplitude and phase) for the example with three propagation paths.

There are two additional parameters limiting the ranging accuracy. The coherence distance is the maximum distance over which an antenna can be moved before the correlation between old and new CIR drops below a given limit. Similarly, the coherence bandwidth is the maximum frequency shift of the signal before the correlation between old and new CTR drops below a given limit. The measurement system bandwidth can be defined using this parameter: for a wideband system, the bandwidth used for ranging is larger than the coherence bandwidth. On the contrary, for a narrowband system, the utilized bandwidth is smaller.

3. Phase-based Ranging Principles

Phase-based ranging methods are able to provide high accuracy of range estimation because of their robustness to the variation of signal strength. Phase measurement in both the time and frequency domain described below has been explored and published in [5], [6].

The range estimation is sensitive to the phase corruption caused by multipath propagation because all these methods are based on narrowband measurements. The problem is depicted in Fig. 5 and Fig. 6. An "instantaneous distance" with respect to measurement frequency has been computed based on the CIR according to:

$$d_{inst} = c \cdot \tau_g \qquad (5)$$

where *c* is the speed of light and τ_g is the group delay:

$$\tau_g = -\frac{d\phi}{d\omega} \approx -\frac{\Delta\phi}{2\pi \cdot \Delta f} \qquad (6)$$

where $\Delta\phi$ is the phase difference between the CTF samples spaced by Δf after phase unwrapping.

We assume an estimator that averages several group delay measurements. For a simple deterministic channel with only two paths, averaging over a large bandwidth works reliably – the difference between the true LOS distance and the estimation is only a few percent. The estimation is always positively biased (higher than LOS) because all the NLOS paths arising from multipath propagation are longer than LOS. For a narrowband measurement, e.g. near 1.15 GHz in Fig. 5, the result may be completely wrong and leads to negative distances.

If we consider a CIR with a large stochastic NLOS part, the range estimation gets significantly biased even using a large averaging bandwidth – the range in Fig. 6 is about two times higher than the true LOS distance. The results from narrowband measurements in such multipath scenarios are therefore purely random.

3.1 Narrowband PDoA with Freq. Hopping

Phase difference of arrival in the frequency domain (FD-PDoA) method is based on a set of measurements at discrete frequencies [7], [8]. The RFID tag must be stationary during the measurement. Bistatic range estimation using linearly spaced measurement frequencies is:

$$d = \frac{c}{2\pi \cdot \Delta f} \cdot \overline{\Delta\phi} - l_{corr} \qquad (7)$$

where $\overline{\Delta\phi}$ is an average of phase change between consequent frequencies. For a monostatic system, the 2π coefficient changes to 4π. The estimation d includes the real distance between reader antennas and the tag, signal propagation delay in RFID front end and antenna cables, and tag backscatter phase offset. The last two components are nearly constant and can be subtracted or calibrated out from the result, leaving the real range estimation itself.

These factors are incorporated in l_{corr} correction distance. The measured correction can be obtained as an average of differences between measured and real distances. It includes the propagation delay on the antenna cable, phase delay caused by the tag reflection (typical value ca. 1 m according to [9]), and various delays of the front end.

The described method is not reliable for complex multipath environments [3, p. 46]. Even if there is a large number of measurement points covering a wide bandwidth, it is still a narrowband measurement – each phase pair gives an independent range estimation, which is averaged later. As a result, only the mean delay τ_0 can be estimated in a multipath environment with a large RMS delay spread τ_{RMS}. This value is therefore always higher than τ_{LOS}.
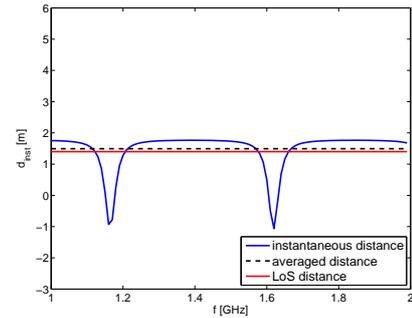
Fig. 5. Distance estimation based on a channel with two paths.
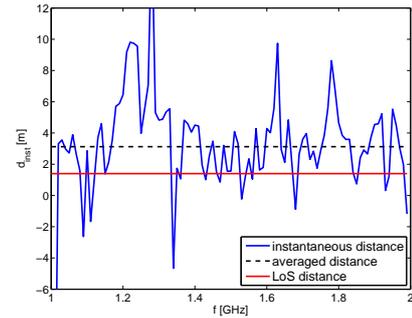
Fig. 6. Distance estimation for stochastic NLOS part of CIR.

4. Channel Models and Simulations

In order to test the performance of current ranging methods and to simplify the development and testing of its derivatives, it is necessary to use an RFID channel simulation tool. Most of the currently used systems are targeted to an analysis of narrowband state-of-the-art RFID setups, without the consideration of pinhole behavior of the channel [10], [11], [12]. Moreover, it is especially important for ranging simulations to include multi-ray propagation with ray folding, otherwise the results are inaccurate.

As a consequence, simulators specialized on channel simulation for ranging are being developed. The most advanced open-source system is the PARIS Simulation Framework, described in [13], [3]. It is a complex MATLAB-based time-domain system-level simulator, which features tag behavioral models and hybrid ray-tracing/stochastic RF propagation channel models. The framework is also very demanding on computational power.

On the other hand, there are several simple simulators based on a deterministic channel, which are easy to understand and use, such as [7]. These systems typically ignore high-order reflections (i.e. all reflections except the first one) and provide only a limited number of rays.

A new RFID channel simulator has been created as a support tool for this paper. The simulation level is basic compared to the PARIS Simulation Framework, but the system is very intuitive and quick to set up. It provides combined deterministic/stochastic wideband modeling with high-order ray folding. Moreover, it is devoted to RFID channels, so it assumes degenerate (pinhole) behavior [14].

4.1 Antenna Placement

Several positioning sites are considered in the following sections. All of them are simplified cases of a real situation, as there are no major obstacles in the measurement area. The simulations include an anechoic chamber (idealized direct LOS propagation with no multipath), open space (direct path and one ray reflected by the floor), ideal room (direct path and multiple rays reflected from all the walls), and common room (modeled as the ideal room with stochastic propagation components). An area with a square-shaped ground plan was selected.

Up to four antennas were placed in the test sites. The placement needs to consider antenna directional characteristics, maximum reading distance, self-interference between the RX and TX path in the reader, and most of all the desired methods of tag localization.

(a) Distance only   (b) Distance and direction
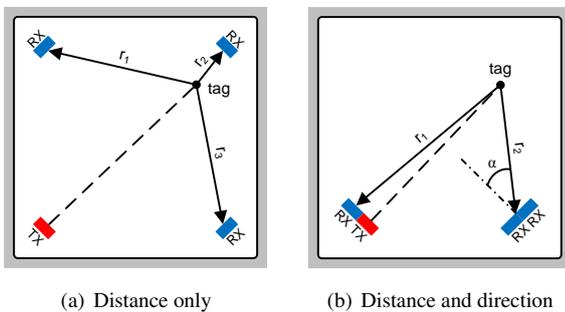
Fig. 7. Antenna placement scenarios for positioning with a set of four antennas.

The first setup is shown in Fig. 7(a). The antennas are placed in each corner of the area. One of the antennas is TX, while the other three are RX, enabling range ellipses measurement. This scenario does not allow direction estimation, however it provides more independent ranging points.

Another setup in Fig. 7(b) can be used for both distance and direction measurement. It consists of two pairs of antennas. The first pair is placed in the lower-left corner, serves for TX and RX, and can be used for ranging. If the antennas in the pair are close enough ($d \ll \lambda$), it is considered to be a monostatic system, thus simplifying the ranging problem from ellipses to circles. The second pair is placed in the lower-right corner and provides two RX antennas. Together with the TX antenna, it allows to perform another independent ranging. Moreover, the two antennas act as an array, and therefore they are able to provide direction-of-arrival (DoA) information. In order to work in such a configuration, the measured tag must be placed in the far field region of the antenna system.

4.2 RFID Channel Emulator

The RFID Channel Emulator (RCHE) is a set of several MATLAB functions that allows computation of the complex CTF for two basic sweeps: over frequency with fixed 3D position, and over 2D position with fixed height and frequency. The structure of the RCHE source files is shown in Fig. 8.
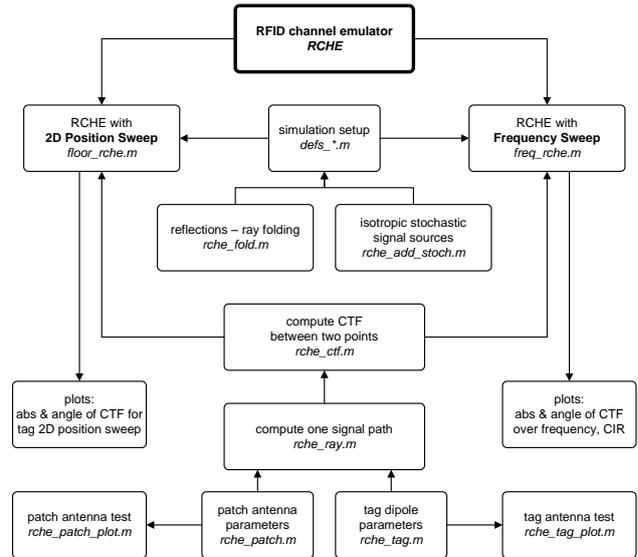
Fig. 8. Structure of RCHE source files. Simulation is performed either with 2D position sweep or with frequency sweep.

The propagation is always simulated on a pinhole channel, i.e. the signal goes from the TX antenna, it is backscattered (received and transmitted) by the tag under test, and received by the RX antenna. The power level of the received signal is checked both on the tag (tag power-on threshold requirement) and on the RX antenna (minimum detectable signal with respect to self-blocking CW).

Each simulation is configured by a definition file. The definitions include:

- TX power in Watts,
- complex tag reflection coefficient,
- complex obstacle reflection (ray folding) coefficient,
- TX and RX antenna positions in 3D space together with antenna bearing (vertical angle is assumed zero),
- room dimensions,
- number of stochastic component sources and the standard deviation of its distribution,
- list of basic (first order) reflections,
- the order of ray folding.

The deterministic simulation can include multiple signal reflections. Every signal path is computed (two complex CTFs for TX–tag and tag–RX) and added together. The stochastic components are modeled using a defined number of isotropic signal sources. Each of these sources has a random position outside the room dimensions and a random power, which is Rayleigh distributed.

Both simulators start with filling the list of possible reflections. This list can include two types of information: a reflector plane definition, and an isotropic source definition. Both ray folding and stochastic generator add new lines into this list. As a result, the list includes all considered reflection planes and stochastic sources.

4.2.1 RCHE with Frequency Sweep

The simulation with frequency sweep requires a defined tag position in 3D space. Frequency sweep is defined by the frequency range and step size. Two complex CTFs are computed, the first one for TX–tag and the second one for tag–RX. The received complex signal at the RX antenna is a product of TX power, CTF between TX–tag, tag reflection coefficient, and CTF between tag–RX. Both the CTFs already include directional antenna gains.

As the last step, the absolute value of CIR is computed using the direct Fourier transform. Fig. 12(b) and Fig. 12(c) show the examples of simulated CTF and CIR, respectively, together with a highlighted point at the real TX–tag–RX distance in CIR. Two additional numerical results are provided: the range estimation based on group delay averaging (see Section 3) and the FFT range estimation based on the first component in the CIR (as described in Section 2).

4.2.2 RCHE with 2D Position Sweep

This type of simulation performs 2D tag position sweep in the X-Y plane. Both antennas are stationary and the tag under test is moved over a 2D mesh. Its height is constant, as well as the measurement frequency. Two CTFs are computed (TX–tag and tag–RX). Much like in the previous simulation, the received complex signal at the RX antenna is a product of TX power, CTF between TX–tag, tag reflection coefficient, and CTF between tag–RX.

Examples of amplitude and phase of the simulated signals are shown in Fig. 9 and Fig. 10. The white color in the images shows the regions where the power level was under the limit – either under the minimum tag power-on threshold or under the minimum detectable signal.

4.3 Simulation Results

The simulations have been processed for several levels of complexity. All of them are simplified cases of a real situation without large obstacles in the measurement area. Frequency was swept from 800 to 1000 MHz with a tag placed at $\vec{p}_{tag} = [3, 4, 0.95]$ m, 2D tag position has been altered over the whole area at 0.95 m height, simulated at 915 MHz.

Channel models with a combination of frequency and position sweeps were applied to the bistatic narrowband FD-PDoA ranging method. Fig. 11 shows the difference between range estimation and true distance (i.e. the ranging error) for each possible tag position. Again, several environment models have been used. The ranging was processed at frequencies from 902 MHz to 928 MHz with a 500 kHz step.

4.3.1 Free Space Deterministic Environment

Free space provides an idealized direct LOS propagation with no multipath. The anechoic RF chamber can be considered as an example of such an environment, despite of some limitations on its parameters (a typical RF chamber

with pyramidal hybrid absorbers [15] has a reflection coefficient of about -20 dB).

The results are shown in Fig. 9(a) and Fig. 10(a). Simulation is based on LOS propagation only, resulting in a Gaussian degenerate channel. Noise is not considered. Both amplitude and phase of received signal are ideally distributed. There is a strong peak in the CIR, representing the range estimation. Moreover, this channel is practically frequency independent even in a wide band scope, as can be seen from the CTF in Fig. 12(a). The FD-PDoA ranging error is zero.

4.3.2 Ground Reflection (Two-ray Deterministic Model)

The two-ray deterministic model adds a ground (floor) reflection into the previous setup with direct ray. Such a model can be used to estimate the ranging performance in places like a building roof, large open spaces, etc. Two- and three-ray models are good for RSS calculation, but still not accurate enough for ranging [3]. Fig. 11(a) shows the ranging error for the two-ray model.

4.3.3 Ideal Room (Multi-ray Deterministic Model)

A multi-ray model consists of a large number of deterministic rays added to the direct path. The rays are created by the reflection from all the walls, floor and ceiling. Only the first and the second order reflections are considered. Such a model approximates an ideal room.

Simulation results are shown in Fig. 9(b) and Fig. 10(b). It can be seen that the amplitude distribution is strongly affected, especially near the reflecting walls. On the other hand, the phase distribution in short range is still very clear.

The ranging error is depicted in Fig. 11(b). The central area between antennas provides reliable ranging estimation (with error below 0.5 m), but there are several small spots with very high predicted error (over 2 m).

4.3.4 Combined Deterministic/Stochastic Model

A combined model adds stochastic components into previous multi-ray simulations. It is an example of an actual room with small obstacles. Stochastic components are modeled using 40 signal sources with a random position outside the room and a Rayleigh distributed power. The number of sources was selected according to the central limit theorem.

The simulations based on the combined model can be found in Fig. 9(c) and Fig. 10(c). Both amplitude and phase of the received signal are affected by multipath. The tag power-on threshold causes random behavior at longer distances. The CTF in Fig. 12(b) strongly depends on frequency and the range peak in the CIR in Fig. 12(c) can be found only if the measurement bandwidth is wide enough.

Fig. 11(c) provides ranging error estimation. Most of the area does not allow narrowband FD-PDoA ranging with error below 2 m, which is unacceptable in most applications. Therefore, a UWB system needs to be used for positioning in such a strong multipath environment.
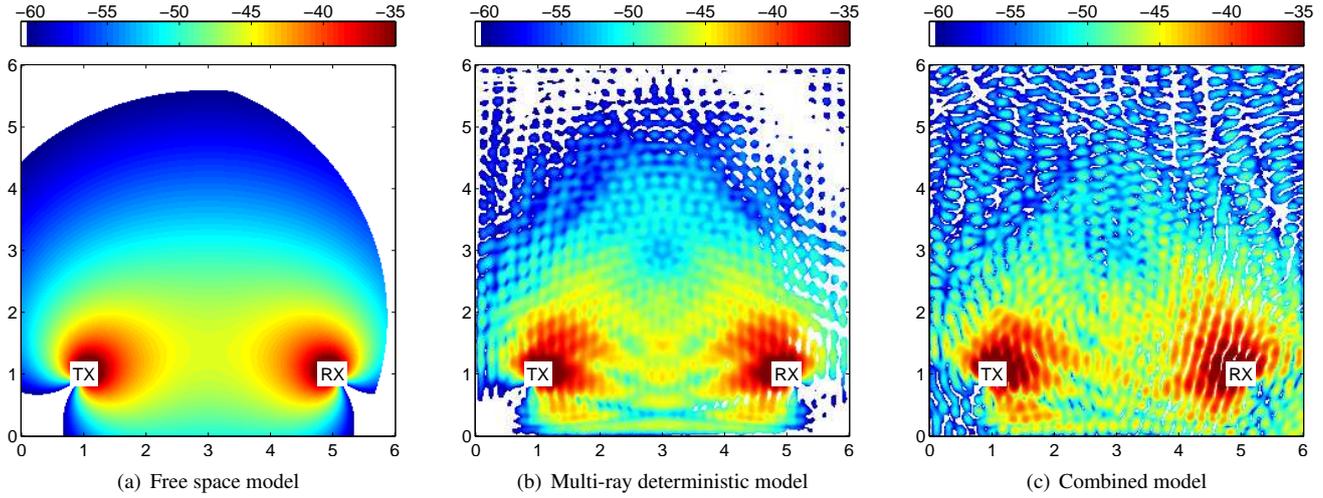
Fig. 9. Simulation results, scenario "Distance and direction", amplitude of received tag signal in [dBm]. Tag position $\vec{p}_{tag} = [x, y, 0.95]$ m is swept over x and y dimensions, antennas at $\vec{p}_{TX} = [1, 1, 1]$ m heading $45°$, $\vec{p}_{RX} = [5, 1, 1]$ m heading $135°$, $P_{TX} = 0.5$ W, $f = 915$ MHz.
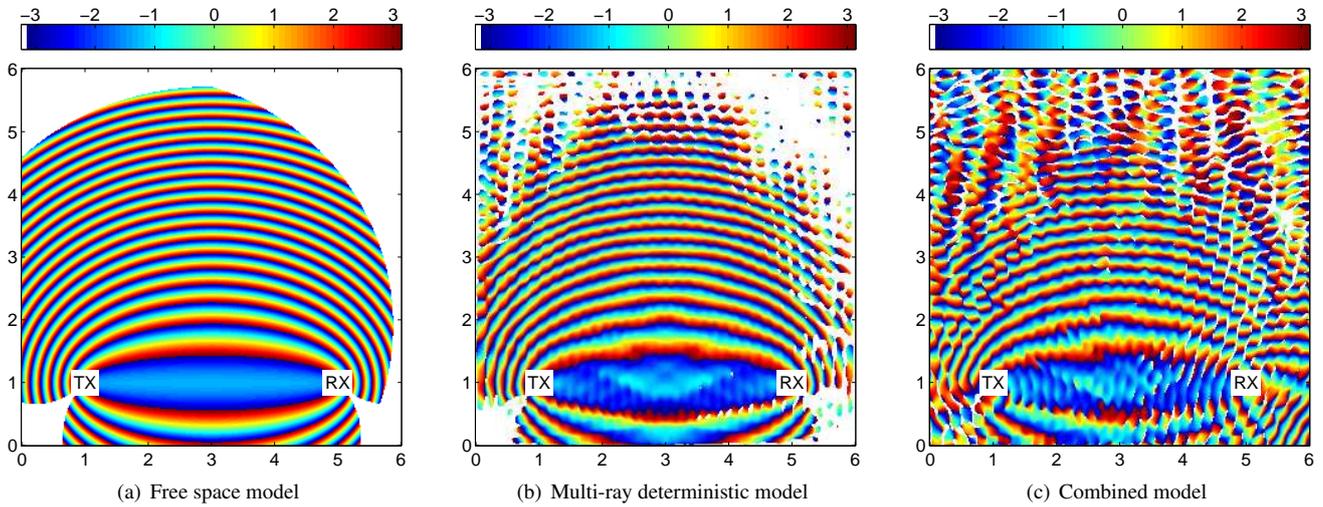
Fig. 10. Simulation results, scenario "Distance and direction", phase of received tag signal in radians. Tag position $\vec{p}_{tag} = [x, y, 0.95]$ m is swept over x and y dimensions, antennas at $\vec{p}_{TX} = [1, 1, 1]$ m heading $45°$, $\vec{p}_{TX} = [5, 1, 1]$ m heading $135°$, $P_{TX} = 0.5$ W, $f = 915$ MHz.
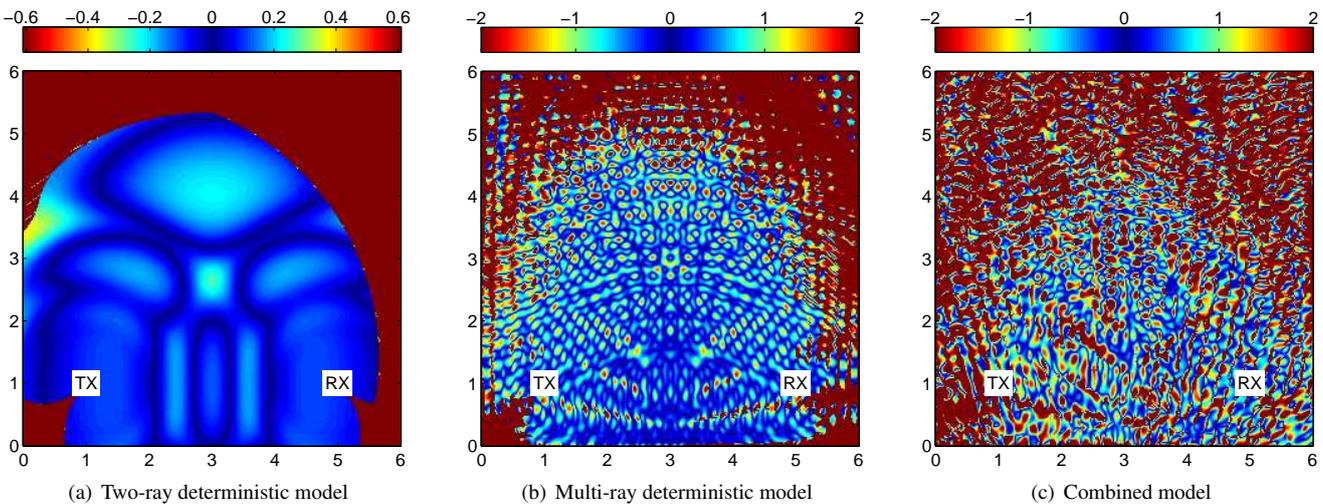
Fig. 11. Simulation results, scenario "Distance and direction", narrowband FD-PDoA distance estimation error in [m]. Tag position $\vec{p}_{tag} = [x, y, 0.95]$ m is swept over x and y dimensions, antennas at $\vec{p}_{TX} = [1, 1, 1]$ m heading $45°$, $\vec{p}_{RX} = [5, 1, 1]$ m heading $135°$, $P_{TX} = 0.5$ W, frequencies according to the US RFID band (50 channels from 902 MHz to 928 MHz with 500 kHz step).

(a) CTF – Free space model   (b) CTF – Combined model   (c) CIR – Combined model
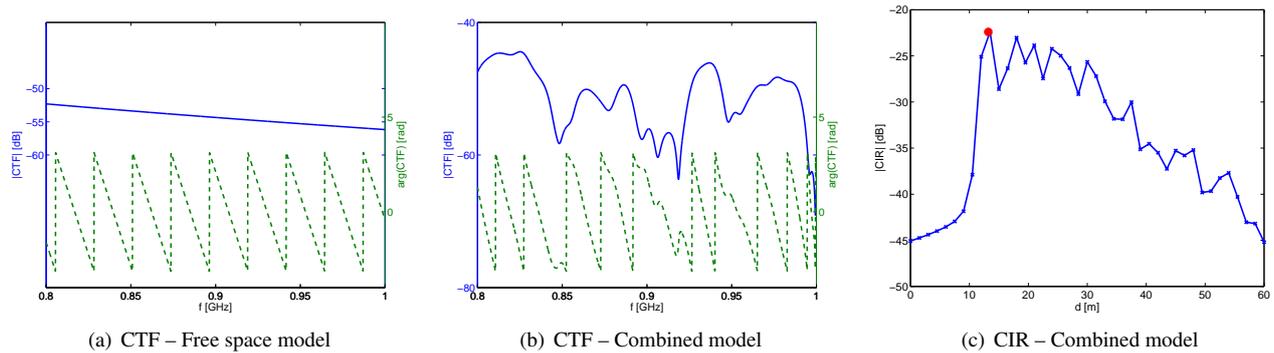
Fig. 12. Simulation results, scenario "Distance and direction", channel transfer function (blue solid – relative amplitude in [dB], green dashed – phase in radians) and channel impulse response (blue solid – relative amplitude in [dB]). Tag position $\vec{p}_{tag} = [3, 4, 0.95]$ m, antennas at $\vec{p}_{TX} = [1, 1, 1]$ m heading $45°$, $\vec{p}_{RX} = [5, 1, 1]$ m heading $135°$, $P_{TX} = 0.5$ W, frequency is swept from 800 to 1000 MHz.

5. Conclusions

In this paper, we have focused on the degenerate wireless channel modeling and simulation with an emphasis on ranging and positioning. The degenerate behavior of the channel in RFID systems leads to specific simulations with stationary transmitter/receiver and moving RFID tag under test.

Several channel models have been proposed and simulated. The results begin with an ideal distribution of amplitude and phase in the free space model (LOS only) and finish with images produced by a combined deterministic/stochastic model with ray folding. Deterministic model simulations have been already confirmed by measurements [6].

The final ranging error simulations for FD-PDoA imply the usability of narrowband methods only for simple environments without severe multipath propagation. Complex real-world scenarios (simulated by a combined deterministic/stochastic model) require a wide bandwidth, which enables range estimation based on impulse response of the wireless channel.

In future work, we would like to verify the ranging error models with measurements on an experimental RFID front end [16], extended to support MISO applications with multiple receiving antennas.

Acknowledgements

References

[1] DOBKIN, D. M. *The RF in RFID: Passive UHF RFID in Practice*. Burlington (MA, USA): Newnes, 2007.

[2] ZHANG, Y., LI, X., AMIN, M. G. Principles and techniques of RFID positioning. BOLIC, M., SIMPLOT-RYL, D., STOJMENOVIC, I. (Eds.) *RFID systems: Research trends and challenges*, ch. 15, p. 389 - 415. Chichester (UK): John Wiley & Sons, 2010.

[3] ARNITZ, D. *Tag Localization in Passive UHF RFID*, PhD thesis. Graz (Austria): Graz University of Technology, 2011. [Online] Cited 2012-01-24. Available at: http://www.spsc.tugraz.at/sites/default/files/phdthesis-arnitz_online.pdf

[4] SAUNDERS, S. R., ZAVALA, A. A. *Antennas and Propagation for Wireless Communication Systems*, 2nd ed. Chichester (UK): John Wiley & Sons, 2007.

[5] POVALAČ, A., ŠEBESTA, J. Phase of arrival ranging method for UHF RFID tags using instantaneous frequency measurement. In *ICECom 2010, Conference Proceedings*. Dubrovnik (Croatia), 2010, p. 1 - 4.

[6] POVALAČ, A., ŠEBESTA, J. Phase difference of arrival distance estimation for RFID tags in frequency domain. In *IEEE International Conference on RFID-Technology and Applications 2011*. Sitges (Spain), 2011, p. 180 - 185.

[7] NIKITIN, P. V., MARTINEZ, R., RAMAMURTHY, S., LELAND, H., SPIESS, G., RAO, K. V. S. Phase based spatial identification of UHF RFID tags. In *Proceedings of the IEEE International Conference on RFID*. Orlando (FL, USA), 2010, p. 102 - 109.

[8] LI, X., ZHANG, Y., AMIN, M. G. Multifrequency-based range estimation of RFID tags. In *Proceedings of the IEEE International Conference on RFID*. Orlando (FL, USA), 2009, p. 147 - 154.

[9] VIIKARI, V., PURSULA, P., JAAKKOLA, K. Ranging of UHF RFID tag using stepped frequency read out. *IEEE Sensors Journal*, 2010, vol. 10, no. 9, p. 1535 - 1539.

[10] DERBEK, V., PREISHUBER-PFLUEGL, J., STEGER, C., PISTAUER, M. Architecture for model-based UHF RFID system design verification. In *European Conference on Circuit Theory and Design (ECCTD'05)*. Cork (Ireland), 2005, vol. 2, p. 181 - 184.

[11] FLOERKEMEIER, C., PAPPU, R. Evaluation of RFIDSim – a physical and logical layer RFID simulation engine. In *Proceedings of the IEEE International Conference on RFID 2008*. Las Vegas (NV, USA), 2008, p. 350 - 356.

[12] DIMITRIOU, A. G., BLETSAS, A., POLYCARPOU, A. C., SAHALOS, J. N. Theoretical findings and measurements on planning a UHF RFID system inside a room. *Radioengineering*, 2011, vol. 20, no. 2, p. 387–397.

[13] ARNITZ, D., MUEHLMANN, U., GIGL, T., WITRISAL, K. Wide-band system-level simulator for passive UHF RFID. In *Proceedings of the IEEE International Conference on RFID*. Orlando (FL, USA), 2009, p. 28 - 33.

[14] PAULRAJ, A., NABAR, R., GORE, D. *Introduction to Space-Time Wireless Communications*. Cambridge (UK): Cambridge University Press, 2003.

[15] Emerson & Cuming Anechoic Chambers NV. *ECCOSORB® VHY-NRL Pyramidal Hybrid Absorber (datasheet)*, 2010.

[16] POVALAČ, A., ŠEBESTA, J. Experimental front end for UHF RFID reader. *Elektrorevue - Journal for Electrical Engineering*, 2011, vol. 2, p. 55 - 59.

About Authors...

Ales POVALAC was born in Trebic in 1985. He received the B.Sc. and M.Sc. degrees in electrical engineering from the Brno University of Technology in 2007 and 2009, respectively. He is currently a Ph.D. student at the Dept. of Radio Electronics, BUT. His research interests are focused on RFID systems working in the UHF band, software defined radio and embedded systems. He is a holder of the Brno PhD Talent Scholarship.

Klaus WITRISAL received the Dipl.-Ing. degree in electrical engineering from Graz University of Technology, Austria, in 1997, the Ph.D. degree (cum laude) from Delft University of Technology, The Netherlands, in 2002, and the Venia Docendi (Habilitation) from Graz University of Technology in 2009. From 1997 till 2001, he was a Ph.D. Student and Research Engineer at Delft University of Technology, and in 2002, he was a Project Leader with AVL in Graz, Austria. Currently, he is an Associate Professor at the Signal Processing and Speech Communication Laboratory (SPSC) of Graz University of Technology. His research interests are in signal processing for broadband and UWB wireless communications, propagation channel modeling, and positioning. He is co-chair of the MTT/COM Society of the IEEE Austria Section.

Jiri SEBESTA was born in Brno in 1973. In 1997, he graduated in Communication Engineering from the Faculty of Electrical Engineering, BUT. In 2005, he obtained his PhD degree in Radio Engineering from the Faculty of Electrical Engineering and Communication, BUT. Currently, he is an associate professor at the same faculty. Since 2008 he has been an IEEE committee member of the Czech-Slovak section. His research interests are in the field of software radio architectures and communication signal processing.